



Measurements of primary trace gases and NO_y composition in Houston, Texas

Winston T. Luke^{a,*}, Paul Kelley^a, Barry L. Lefer^b, James Flynn^b, Bernhard Rappenglück^b, Michael Leuchner^{b,1}, Jack E. Dibb^c, Luke D. Ziemba^c, Casey H. Anderson^c, Martin Buhr^d

^a National Oceanic and Atmospheric Administration, Air Resources Laboratory, Silver Spring, MD, USA

^b Department of Earth and Atmospheric Sciences, University of Houston, Houston, TX, USA

^c Institute for the Study of Earth, Oceans, and Space, Climate Change Research Center, University of New Hampshire, Durham, NH, USA

^d Air Quality Design, Inc., Golden, CO, USA

ARTICLE INFO

Article history:

Received 12 November 2008

Received in revised form

18 August 2009

Accepted 19 August 2009

Keywords:

NO_y budget

Ozone photochemistry

Air quality

Sulfur dioxide

Carbon monoxide

Houston

TEXAQS-II

ABSTRACT

Concentrations of CO, SO₂, NO, NO₂, and NO_y were measured atop the University of Houston's Moody Tower supersite during the 2006 TexAQS-II Radical and Aerosol Measurement Project (TRAMP). The lowest concentrations of all primary and secondary species were observed in clean marine air in southerly flow. SO₂ concentrations were usually low, but increased dramatically in sporadic midday plumes advected from sources in the Houston Ship Channel (HSC), located NE of the site. Concentrations of CO and NO_x displayed large diurnal variations in keeping with their co-emission by mobile sources in the Houston Metropolitan Area (HMA). CO/NO_x emission ratios of 5.81 ± 0.94 were observed in the morning rush hour. Nighttime concentrations of NO_x (NO_x = NO + NO₂) and NO_y (NO_y = NO + NO₂ + NO₃ + HNO₃ + HONO + 2*N₂O₅ + HO₂NO₂ + PANs + RONO₂ + p-NO₃ + ...) were highest in winds from the NNW-NE due to emission from mobile sources. Median ratios of NO_x/NO_y were approximately 0.9 overnight, reflecting the persistence and/or generation of NO_z (NO_z = NO_y - NO_x) species in the nighttime Houston boundary layer, and approached unity in the morning rush hour. Daytime concentrations of NO_x and NO_y were highest in winds from the HSC. NO_x/NO_y ratios reached their minimum values (median ca 0.63) from 1300 to 1500 CST, near local solar noon, and air masses often retained enough NO_x to sustain additional O₃ formation farther downwind. HNO₃ and PANs comprised the dominant NO_z species in the HMA, and on a median basis represented 17–20% and 12–15% of NO_y, respectively, at midday. Concentrations of HNO₃, PANs, and NO_z, and fractional contributions of these species to NO_y, were at a maximum in NE flow, reflecting the source strength and reactivity of precursor emissions in the HSC. As a result, daytime O₃ concentrations were highest in air masses with HSC influence. Overall, our findings confirm the impact of the HSC as a dominant source region within the HMA. A comparison of total NO_y measurements with the sum of measured NO_y species (NO_{yi} = NO_x + HNO₃ + PANs + HONO + p-NO₃) yielded excellent overall agreement during both day ([NO_y](ppb) = ([NO_{yi}](ppb))*1.03 ± 0.16) - 0.42; r² = 0.9933) and night ([NO_y](ppb) = ([NO_{yi}](ppb))*1.01 ± 0.16) + 0.18; r² = 0.9975). A similar comparison between NO_y-NO_x concentrations and the sum of NO_{zi} (NO_{zi} = HNO₃ + PANs + HONO + p-NO₃) yielded good overall agreement during the day ([NO_z](ppb) = ([NO_{zi}](ppb))*1.01 ± 0.30) + 0.044 ppb; r² = 0.8527) and at night ([NO_z](ppb) = ([NO_{zi}](ppb))*1.12 ± 0.69) + 0.16 ppb; r² = 0.6899). Median ratios of NO_z/NO_{zi} were near unity during daylight hours but increased to approximately 1.2 overnight, a difference of 0.15–0.50 ppb. Differences between NO_z and NO_{zi} rarely exceeded combined measurement uncertainties, and variations in NO_z/NO_{zi} ratios may have resulted solely from errors in conversion efficiencies of NO_y species and changes in NO_y composition. However, nighttime NO_z/NO_{zi} ratios and the magnitude of NO_z - NO_{zi} differences were generally consistent with recent observations of ClNO₂ in the nocturnal Houston boundary layer.

Published by Elsevier Ltd.

1. Introduction

The 2000 Texas Air Quality Study (TEXAQS-2000) was conducted in and around the Houston Metropolitan Area (HMA) in August–September 2000 to investigate the causes of Houston's repeated non-attainment of federal air quality standards. A major finding of

* Corresponding author. Tel.: +1 (301) 713 0971; fax: +1 (301) 713 0119.

E-mail address: Winston.Luke@noaa.gov (W.T. Luke).

¹ Now at: Fachgebiet für Ökologiklimatologie, Technische Universität München, Freising, Germany.

TEXAQS-2000 documented the unusually large abundance of highly reactive volatile organic compounds (HRVOCs) in the Houston atmosphere and their role in the rapid and efficient photochemical generation of O₃ in the region (e.g., Ryerson et al., 2003; Jiang and Fast, 2004; Daum et al., 2003, 2004; Kleinman et al., 2002). The second Texas Air Quality study (TexAQS-II) was conducted from January 2005 to December 2006 and was designed to document and assess changes to air quality in southeastern Texas since 2000. The TexAQS-II Radical and Aerosol Measurement Project (TRAMP) was conducted at the North Moody Tower “supersite” on the campus of the University of Houston as part of the intensive operations period within TEXAQS-II. The background and objectives of TRAMP have been reviewed in Cowling et al. (2007) and Lefer et al. (in this issue).

The link between O₃ and NO_x (NO_x = NO + NO₂) photochemistry has been extensively studied for decades. The fundamental characteristics of urban photochemistry are reviewed by Finlayson-Pitts and Pitts (2000) and references therein, and are described in relation to Houston's unique chemical and meteorological environment by Flynn et al. (in this issue), Lefer et al. (in this issue), and Cowling et al. (2007). Briefly, net ozone production occurs when peroxy radicals (RO₂), formed from photochemical reactions involving the hydroxyl radical (OH) with VOCs, oxidize NO to NO₂. Subsequent photolysis of NO₂ liberates an O(³P) atom, which reacts with O₂ to form O₃, and NO, which can go on to generate additional O₃ by repeated reactions with RO₂. Photochemical ozone generation is constrained by the competition for NO_x between reactions which perpetuate the catalytic cycle of NO–NO₂–O₃ reactions and those which terminate that cycle by converting NO₂ to nitric acid (HNO₃). Interactions of organic free radicals with NO₂ can produce peroxyacetyl nitrate (PAN) and its homologues, but these species are thermally unstable and typically act as temporary reservoirs of NO_x in the lower atmosphere. Nighttime reactions can generate other species such as nitrate radical (NO₃), nitrous acid (HONO), nitric acid anhydride (N₂O₅) and nitryl chloride (ClNO₂), the latter particularly in a marine environment (Osthoff et al., 2008). These species can liberate NO, OH radicals, and/or Cl radicals upon photolysis the following morning, thereby contributing to the daytime photochemical cycle.

Comparisons of measurements of total NO_y (NO_y = NO + NO₂ + NO₃ + HONO + 2*N₂O₅ + HO₂NO₂ + PANs + RONO₂ + p-NO₃ + ...) with the sum of individually measured component species constitute an important assessment of our ability to properly measure reactive nitrogen species and to close the reactive nitrogen budget. Such studies have been used to identify potentially important “missing” NO_y compounds which may not be adequately measured by current analytical methods (Fahey et al., 1986; Buhr et al., 1990; Williams et al., 1997). Neuman et al. (2002) evaluated NO_y composition as measured aboard the NOAA WP-3D aircraft during TEXAQS-2000 and found that the measured sum of NO_x, HNO₃, and PAN concentrations agreed with those of total NO_y to within the combined uncertainties of the techniques.

In this paper we discuss measurements of primary trace gases (SO₂, CO, NO, NO₂, NO_y) with regard to local source regions. Observations are classified with respect to time of day and emission source regions inferred from wind direction data. Observations are used to derive CO/NO_x emission ratios from local sources; to identify potential local emission sources and source regions; and to assess the NO_y budget at the Moody Tower supersite.

2. Experimental

Measurements of CO, SO₂, and reactive nitrogen compounds were made from August 15 to October 2, 2006 as part of the NOAA/Air Resources Laboratory's contribution to the TRAMP study. The inlet systems were mounted in a weather-tight NEMA enclosure at the top of a 10 m walk-up scaffold erected on the roof balcony of the

North Moody Tower (MT: 29.718 °N, –95.341 °W) on the University of Houston (UH) campus. The measurement site is described in more detail in Lefer et al. (in this issue). By virtue of its sampling height (70 m above ground level) the site is more representative of emission sources in the wider HMA than of local street-level emissions. The MT site is located approximately 5 km SE of “downtown” Houston, 1 km SW of Interstate 45, and 3.5 km north of the South I-610 loop. The site is positioned 6 km SW and 25 km WSW, respectively, of the western and eastern edges of the petrochemical facilities in the Houston Ship Channel (HSC).

Detailed discussions of the instrumentation deployed in TRAMP appear in Luke et al. (2007) and will be only briefly reviewed here. The trace gas instruments were housed in an air conditioned trailer at the base of the walk-up scaffold. Heated (40 °C) and insulated PFA Teflon[®] tubing was used for all calibration and sampling lines, and all instruments were calibrated at the inlet tip. Sampling lines were protected from particulate contamination with Teflon[®] or other filter elements. Dynamic calibration gas mixtures were generated from NIST-traceable compressed gas standards in an excess flow of humidified zero air (all gases supplied by Scott Marrin, Inc., Riverside CA) using calibrated mass flow controllers (MFCs: Tylan General, Torrance, CA). Labview 8.0 software (National Instruments, Austin, TX) was used for data logging and instrument and calibration control. Analog signals were sampled at 5 s intervals; reduced output data were averaged over 1 min and 1 h time intervals.

2.1. Carbon monoxide, sulfur dioxide, and ozone

The CO and SO₂ detectors shared a common inlet and the combined sample flow passed through a Nafion dryer membrane (Model PD-625-24AFS, Perma Pure Inc., Toms River, NJ) to avoid condensation inside the trailer. Carbon monoxide was measured with a commercial non-dispersive infrared (NDIR), gas filter correlation spectrometer (Model 48S, Thermo Electron Corporation, Waltham, MA) modified for high sensitivity (Dickerson and Delany, 1988; Parrish et al., 1994). Sulfur dioxide was measured with a modified commercial pulsed fluorescence detector (Model 43S, Thermo Electron Corp.) (Luke, 1997; Luke et al., 2007). The CO and SO₂ detectors were calibrated every 1–3 days at concentrations of approximately 1000 and 60 ppb, respectively.

The uncertainty for 1 h average concentrations is estimated to be ±(0.07 ppb + 6% of reported concentration) for SO₂ and ±(10 ppb + 5% of reported concentration) for CO. Hourly averaged CO concentrations measured with the NOAA instrument agreed to within 3.0% of those reported by UH's independent NDIR detector (Model 48C-TLE, Thermo Electron Corp.). The intercept of the regression was 2.0 ppb, and correlation between the detectors was excellent ($r^2 = 0.9870$). The contents of the NOAA CO calibration standard agreed to within 0.2 and 3.8% of two independent UH standards, respectively. Ozone concentrations were measured by scientists from UH using a commercial Thermo Electron Model 49C UV photometric detector. The uncertainty in O₃ concentrations is estimated to be the larger of ±5% or ± 2 ppb.

2.2. Oxides of nitrogen (NO, NO_x, NO_y)

Reactive nitrogen compounds (NO, NO_x, NO_y) were measured with a two-channel ozone chemiluminescence detector. Major components of the NOAA-constructed detector were removed from two commercial detectors (Model 42S, Thermo Electron Corp.) and repackaged into a single enclosure. The limit of detection (LOD) was 0.03 ppb NO (signal to noise ratio 2:1) for a 1 min integration time and was achieved by using a high-output silent-discharge ozone electrode (Ozonology, Inc., Northbrook, IL) and a high capacity Teflon diaphragm pump (DTC-120, Kurt J. Lesker Co., Clairton, PA).

A heated (350 °C) commercial molybdenum converter (Thermo Electron Corp.) was used to measure NO_y continuously on the first channel. The converter was mounted in the NEMA enclosure to minimize adsorptive losses of NO_y species. A MFC immediately downstream of the converter and protected from particulate contamination with a 60 μm mesh stainless steel filter maintained sample flow at 1 standard liter per minute (slm). NO and NO_x were measured sequentially on the second detector channel using a photolytic converter mated to a separate inlet system and MFC. The converter was powered on and off at 1 min intervals with NO₂ determined by difference. The design was based upon that of a solid-state light source converter (US Patent 7,238,328) developed by Air Quality Design, Inc. (Golden, CO). The NOAA converter consisted of a 225 cm³ cylindrical quartz cell illuminated longitudinally with 2 UV LED arrays ($\lambda_{\text{max}} = 395 \pm 5$ nm; Opto Diode Corp., Newbury Park, CA) at each end. A custom power supply provided current control and thermal overload protection to each array. Highly reflective Teflon[®] (Gigahertz-Optik Inc., Newburyport, MA) was used on the outer cell surfaces to enhance photon reflectivity. At the normal sample flow of 1.5 slm and pressure of 100 torr, cell residence time was approximately 1.2 s; correction of NO and NO₂ values for variations in ambient O₃ (e.g., Ridley et al., 1988) was not necessary.

Potential interferences to the LED photolytic technique are few. Only nitrous acid (HONO) has an appreciable absorption cross section near 395 nm; its photolysis potential (the product of the absorption cross section and photolysis quantum yield) is only 1.4% of that of NO₂, but can be an order of magnitude larger at 385–390 nm. The maximum interference posed by N₂O₅ is 0.03% of NO₂, assuming a quantum yield of 1.0 for the photolytic production of NO₂^{*} and subsequent dissociation to NO (Finlayson-Pitts and Pitts (2000), and references therein). Artifact NO₂ formation arising from the thermal decomposition of PAN, N₂O₅, and HO₂NO₂ should be negligible; the LED arrays impart little or no radiant heating to the quartz cell, and temperatures inside the converter were typically at or below outside (ambient) temperatures. PAN decomposition in the heated sample line was deemed to be negligible.

The NO/NO_x/NO_y detector was calibrated automatically every 11 h, and converter artifact levels were determined from extensive zero air flushes prior to calibration. Conversion efficiencies (CE) were measured by periodic gas phase titrations (GPT; Stedman, 1976) and verified frequently by calibrating with NO₂. The NO₂ CE of the molybdenum converter was $97.6 \pm 0.6\%$, while that of the photolytic converter decayed from 56.2% to 51.7% during the study. The NOAA NO calibration standard agreed to within 2.5% of an independent UH standard. The overall uncertainties in hourly averages of NO, NO₂, and NO_y are $\pm(0.015 \text{ ppb} + 7\% \text{ of reported concentration})$, $\pm(0.040 \text{ ppb} + 12\% \text{ of reported concentration})$, and $\pm(0.22 \text{ ppb} + 10\% \text{ of reported concentration})$, respectively.

2.3. Other reactive nitrogen species

Concentrations of NO_y component species are discussed below in the context of NO_y budget studies. Concentrations of peroxyacetyl nitrate (PAN), peroxyacryloyl nitrate (APAN), peroxypropionyl nitrate (PPN), peroxyisobutyryl nitrate (PiBN), and peroxyethacryloyl nitrate (MPAN) were measured at 10 min intervals by UH using an automated GC/ECD technique (Leuchner and Rappenglück, in this issue; Rappenglück et al., submitted for publication). Measurement uncertainties are the larger of $\pm 11.6\%$ or ± 30 ppt for PAN and PPN; $\pm 12.3\%$ or ± 85 ppt for PiBN; $\pm 12.6\%$ or ± 100 ppt for MPAN; and $\pm 22.3\%$ or ± 40 ppt for APAN. The University of New Hampshire (UNH) measured HONO and HNO₃ at 5–10 min intervals using an automated mist chamber technique with ion chromatographic detection (Ziemba et al., in this issue; Stutz et al., in this issue-a). Overall uncertainties of both measurements are $\pm 10\%$. Aerosol

nitrate in particles smaller than 1 μm vacuum aerodynamic diameter was measured with an Aerodyne Research, Inc. (Billerica, MA) quadrupole mass spectrometer (Ziemba et al., in this issue); mass loadings were reported at 10 min intervals with an uncertainty of $\pm 10\%$.

3. Results

The magnitude, variety, and geographical distribution of emission sources in the HMA complicate any analysis of observations there. Numerous petrochemical and other industrial facilities are found to the east of the MT site in the HSC, a region which dominates the emissions of NO_x and VOCs in the metropolitan area (Daum et al., 2003, 2004; Ryerson et al., 2003; Leuchner and Rappenglück, in this issue; Cowling et al., 2007 and references therein). The numerous tanker and cargo ships in the HSC and turning basin emit NO_x, CO, SO₂, and carbonaceous aerosols to the HMA (e.g., Lack et al., 2008; Cowling et al., 2007; Williams et al., in press). Refineries and other industrial sources are located farther a field to the east and southeast in the Beaumont-Port Arthur and Texas City areas, respectively. The 3800 MW W.A. Parish electrical generating unit (EGU), approximately 35 km southwest of the Moody Tower, burns coal and natural gas. Its total net generating capacity is among the largest of all fossil fuel plants in the U.S. (data available at: <http://www.eia.doe.gov/ncic/rankings/plantsbycapacity.htm>) and the plant emits approximately 5000 tons NO_x per year (data available at: <http://www.epa.gov/cleanenergy/energy-resources/egrid/index.html>). Numerous smaller EGUs are located well to the north of Houston. Finally, a series of interstate highways and heavily traveled main roads ring the city and the MT site.

Time series plots of measured CO, SO₂, and NO_y appear in Fig. 1a–c and reflect the complexity of emissions in an urban environment. Emissions from local sources were superimposed on background concentrations which varied with wind direction and upwind emission source intensity. The prevailing meteorology during TRAMP is reviewed in Lefer et al. (in this issue). During the 6-week study, winds were typically from the eastern sector (39.5% from the NE, 27.6% from the SE) with westerly winds less frequent (6.6% from the NW, 26.3% from the SW). Low concentrations of primary and secondary trace species, as well as increased cloud cover and precipitation, were observed in clean southerly flow from the Gulf of Mexico from August 25–28, Sept. 15–18, and Sept. 22–23 (Lefer et al., in this issue). Higher concentrations were measured following frontal passage in the area (Rappenglück et al., submitted for publication), when persistent northerly winds transported natural (biomass burning) and anthropogenic (point-source and urban) emissions from upwind continental sources into the HMA. Under these conditions, local emissions were superimposed on a background of elevated concentrations of CO, SO₂, and reactive nitrogen species, as may be seen by inspection of Fig. 1 a–c. Recirculation of polluted air in the land-breeze/gulf-breeze circulation under weak synoptic flow was responsible for elevated O₃ observed on August 31–Sept. 1, and on Sept. 7, 12, and 26 (Lefer et al., in this issue; Rappenglück et al., submitted for publication).

A summary of the trace gas observations, segregated into day (0800–2000 CST) and night (2000–0800) time periods, appears in Table 1. Median concentrations were typically higher at night in the shallow nocturnal boundary layer (BL); during the day, convective mixing increased BL heights and diluted emissions throughout a larger volume of the lower troposphere (Day et al., in this issue). Fumigation of the Moody Tower by SO₂-rich plumes; titration of NO by O₃ at night; and photochemical generation of NO_x oxidation products (NO_z) account for the observations of higher concentrations of SO₂, NO, and NO_z, respectively, during the daytime (Table 1).

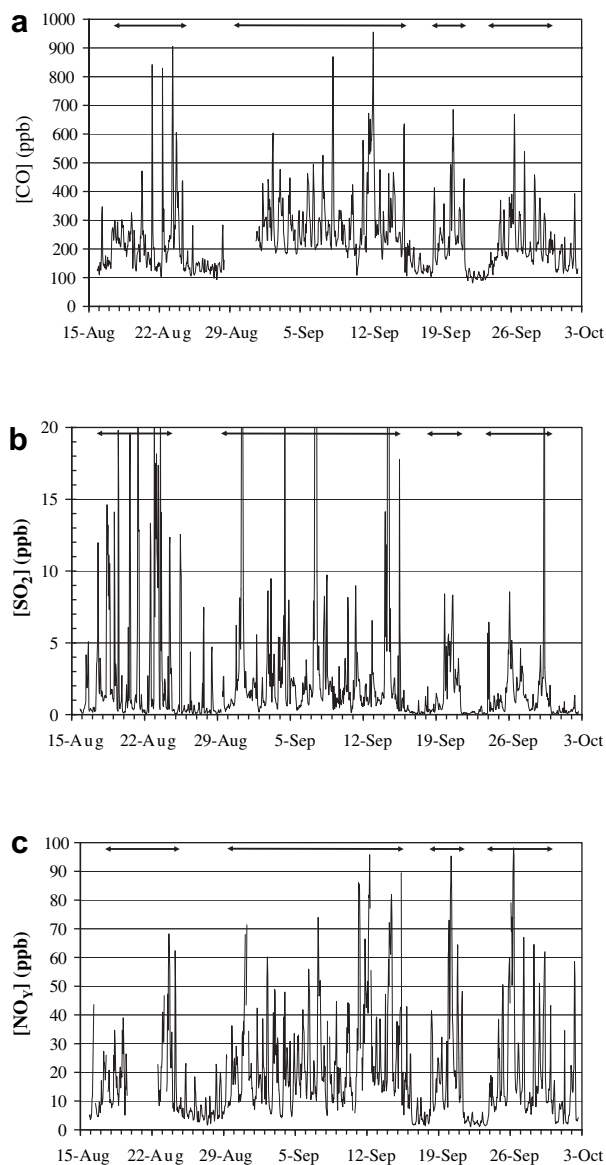


Fig. 1. Time series plots of species concentrations (ppb) during the TRAMP campaign: (a) CO, (b) SO₂, (c) NO_y. Note that the ordinate scale of the SO₂ plot has been expanded. Time periods of enhanced background concentrations are denoted by the horizontal lines at the top of each plot.

Note that the morning rush hour, assumed to be from 0500 to 0900 CST, spanned both day and nighttime periods.

3.1. Carbon monoxide

Median CO concentrations displayed a well defined diurnal variation, increasing during the morning rush hour and peaking at 346 ppb at 0700–0800 CST over all days of the study. Weekdays (Fig. 2a) exhibited a more pronounced diurnal variation than weekends (Fig. 2b) due to higher traffic volumes and greater regularity in variations of traffic density. Between 0600 and 0700 CST median [CO] peaked at 432 ppb during the week, but only at 250 ppb on the weekends. CO typically remained near or below 200 ppb throughout the day on weekends.

A histogram of CO concentrations (not shown) displayed a bimodal distribution, with a mode at 120–140 ppb and a secondary peak at 180–200 ppb. The lowest concentrations of CO, SO₂ and reactive

nitrogen compounds were observed in southerly flow. Day and nighttime CO concentrations were highest in winds from the NW-NE (ca 315°–45°) and were well correlated with NO_x, likely reflecting the co-emission of CO and NO_x in the morning rush hour from mobile sources travelling the interstate highways and arterial roads north of campus. This interpretation is supported by a source apportionment study of VOC compounds measured during TRAMP (Leuchner and Rappenglück, in this issue), which found that the source factor associated with vehicular emissions was elevated in winds from all northerly directions, from the west through the ENE. Northerly winds also brought continental emissions into the HMA. Overall correlation of NO_x and CO concentrations from all wind sectors, day and night, was quite good ($r^2 = 0.7253$).

3.2. Sulfur dioxide

Concentrations of SO₂ in the HMA were typically low; 597 of 1058 hourly averaged values were between 0 and 1 ppb. While median concentrations exhibited little diurnal variation (Fig. 3), inspection of 95th percentile concentrations reveals the occasional impact of SO₂-rich plumes at the site, usually during midday. This behavior is also evident from inspection of Fig. 1b; SO₂ concentrations were usually quite low but were occasionally perturbed by large increases in short-duration plume events. The highest SO₂ concentrations were observed from 0600 to 1400 CST in winds influenced by emissions in the HSC (50°–110°; henceforth referred to as “NE flow”), although high [SO₂] was also occasionally observed at night in winds from this sector; daytime and nighttime [SO₂] averaged 9.31 ± 12.9 ppb in NE flow. Overall, correlation between CO and SO₂ in these air masses was good ($r^2 = 0.6131$) only at SO₂ concentrations exceeding 10 ppb. SO₂/NO_x ratios in NE flow averaged 0.438 ± 0.429 (max = 2.20), considerably higher than the ratio of 0.1–0.15 observed in winds from almost all other sectors. These observations begin to reflect the complex distribution of sources in the HSC; sporadic or episodic primary emissions from co-located or closely located sources in the HSC; and/or the occasional fumigation of the site by specific sources within the HSC possessing unique emissions characteristics.

Elevated SO₂ concentrations were also measured during the day in southwesterly flow (220°–240°). In these air masses, high SO₂ (>4 ppb) correlated well with NO_x ($r^2 = 0.4706$) but not with CO ($r^2 = 0.0790$), which remained low and relatively invariant (161 ± 41 ppb). SO₂/NO_x ratios averaged 0.393 ± 0.773 (max 3.27) in winds from 220° to 240°, suggesting an emissions signature from EGUs southwest of the city (e.g., W.A Parish). Elevated SO₂/NO_x ratios were not observed in SW winds at night, however.

3.3. Reactive nitrogen compounds

Diurnal profiles of weekday NO, NO₂, and NO_y concentrations are shown in Fig. 4a–c, and like CO exhibited clear variations, with concentrations increasing dramatically during the morning rush hour. The growth of the convective BL in mid-late morning, coupled with enhanced photochemical transformations and depositional losses, acted to decrease concentrations throughout the day. Concentrations increased again at night, as late day and nighttime emissions were injected into the smaller volume of the nocturnal BL. Like CO, diurnal variations of [NO_x] and [NO_y] were much smaller on weekends than during the week (Figs. 4 and 5). Concentrations of NO were often near zero at night due to rapid oxidation by O₃ and conversion to NO₂. However, occasional early morning (0300–0500 CST) releases of large amounts of NO from sources in the HSC were advected to the site in NE flow. These perturbations may be seen in Figs. 4a and 5a through examination of 75th and 95th percentile concentrations.

Table 1
Statistics of day and night trace gas observations. All concentrations are in parts per billion by volume (ppb).

	CO		SO ₂		NO		NO ₂		NO _x		NO _y		NO _z	
	Day	Night	Day	Night	Day	Night	Day	Night	Day	Night	Day	Night	Day	Night
Average	209.78	257.35	3.16	1.82	2.43	5.45	9.75	16.63	12.14	21.87	14.80	23.18	2.95	2.06
Std. Deviation	91.42	138.11	7.65	2.78	5.09	12.56	9.73	11.97	13.36	19.76	13.60	19.49	2.91	1.71
Median	194.91	226.43	0.96	0.90	0.94	0.38	6.88	13.38	8.08	15.29	11.28	17.26	2.25	1.83
5th Percentile	109.14	112.11	0.07	0.07	0.10	0.03	1.20	3.05	1.69	3.15	2.27	3.31	0.07	0.03
25th Percentile	142.26	155.36	0.33	0.31	0.42	0.10	3.24	6.86	4.30	7.10	6.07	8.66	0.92	0.58
75th Percentile	243.39	314.06	2.49	2.07	2.11	3.50	11.75	23.18	14.19	30.69	18.26	32.28	4.00	3.13
95th Percentile	394.44	540.69	12.82	6.82	11.00	29.37	30.97	40.01	40.20	66.83	42.08	64.66	8.50	5.06

At night, concentrations of NO_x and NO_y were highest in winds from the NNW-NE due to mobile source emissions in the morning rush hour (e.g., Leuchner and Rappenglück, in this issue). Emissions from upwind continental sources may also have contributed to increased background concentrations of NO_x and NO_y in northerly flow, but this contribution was likely much smaller than for CO due to the shorter atmospheric lifetimes of reactive nitrogen compounds. SO₂/NO_x ratios averaged only about 0.1 in winds from 300° to 40°, suggesting that emission signatures from distant (ca 100 km) EGUs to the north of the HMA were not discernible.

Highest daytime concentrations of NO_x and NO_y were observed in winds from the HSC. Source apportionment analysis (Leuchner and Rappenglück, in this issue) confirmed that the HSC is the

dominant source region for VOC emissions to the HMA, and large VOC and NO_x emissions from petrochemical and other industrial facilities in the HSC have been well documented (e.g., Ryerson et al., 2003; Daum et al., 2003, 2004; Kleinman et al., 2002; Cowling et al., 2007 and references therein). Substantial NO_x is also emitted in the diesel exhaust of tanker and cargo ships in the ship channel (Cowling et al., 2007; Williams et al., in press).

NO_x concentrations were also elevated in winds from the southeast during the day and night. VOC composition reflected a variety of contributing source factors in SE flow, including biogenic emissions, fuel evaporation, vehicular exhaust, aromatic compounds, and natural gas and crude oil signatures. Mobile source emissions from the I-45 and South I-610 loop dominated the VOC emission signatures in SE flow, however, and refinery and other industrial emissions were less important (Leuchner and Rappenglück, in this issue). NO_y concentrations were poorly correlated with the moderate levels of SO₂ measured in SE flow (slope = 0.0388, $r^2 = 0.0261$), but were much better correlated with CO (slope = 5.123, $r^2 = 0.4394$), consistent with a mobile emission source.

NO_x and NO_y concentrations were slightly elevated in winds from the southwest, likely due to daytime emissions from upwind EGUs. Although relatively few observations were made under westerly flow, NO_x and NO_y concentrations were elevated in a broad sector from the SW-NW during the day, most likely from mobile source emissions (I-59, 288, Galleria area, Medical Center) without overlap of industrial sources. Concentrations of NO_x and NO_y were at a minimum in marine air in southerly flow.

3.4. NO_x-CO correlations

The correlation of CO and NO_x concentrations in the morning rush hour has been commonly used as a robust measure of molar

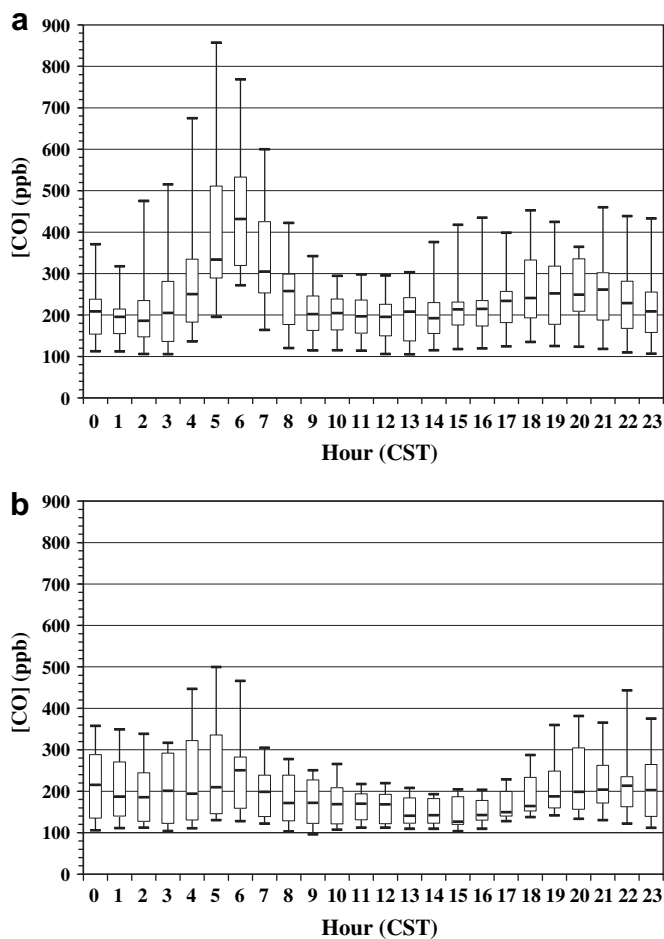


Fig. 2. Diurnal profiles of CO concentration (ppb): (a) weekday aggregated data, (b) weekend data. Horizontal bars represent median concentrations, rectangular boxes denote 25th and 75th percentile concentrations, and whiskers denote 5th and 95th percentile concentrations.

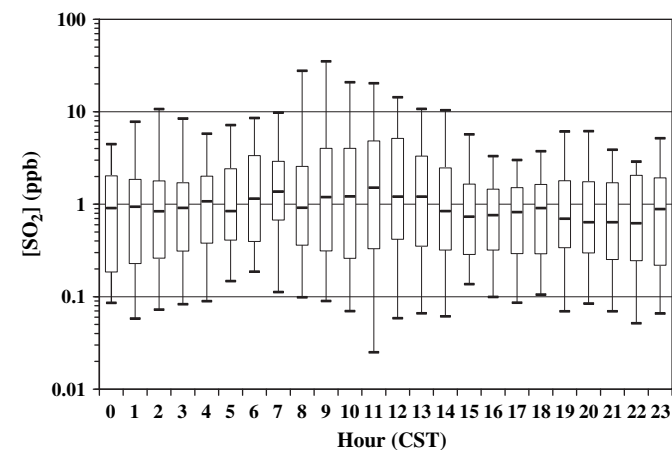


Fig. 3. Same as Fig. 2, for all weekday and weekend SO₂ data (ppb). Note that the concentration scale is logarithmic.

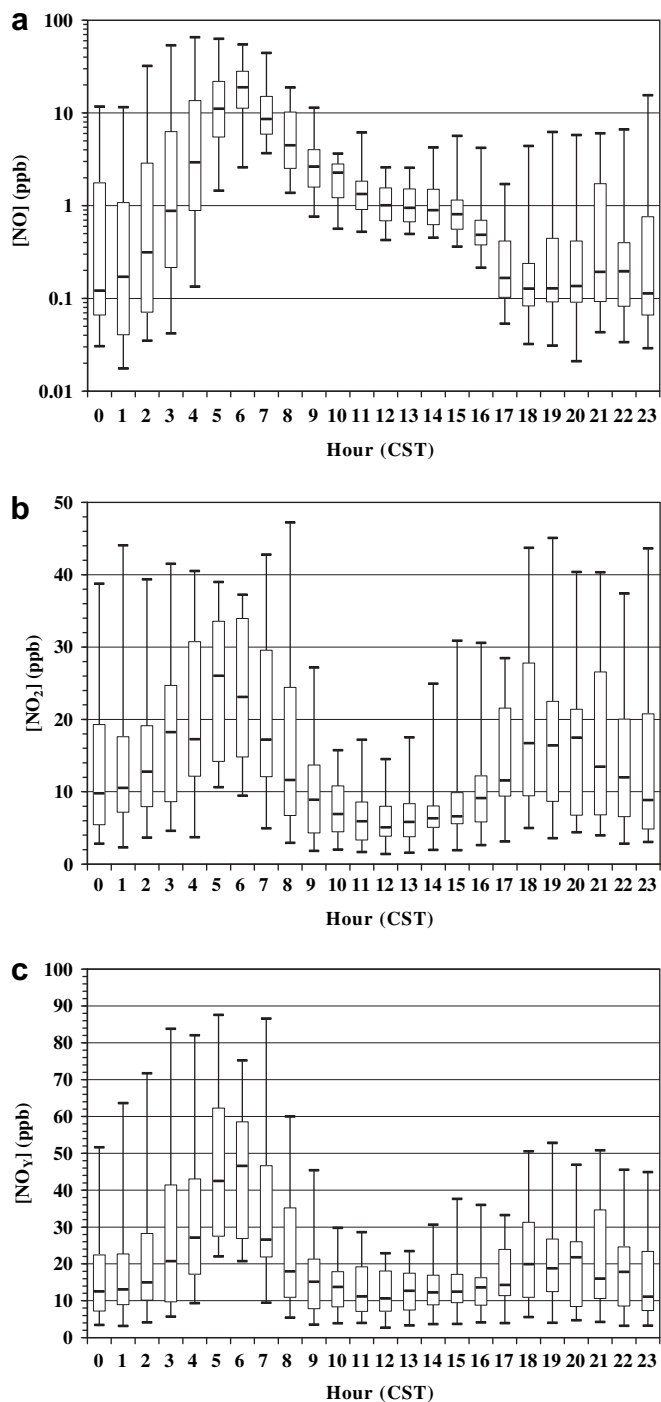


Fig. 4. Same as Fig. 2 for weekday data only: (a) NO (ppb), (b) NO₂ (ppb), (c) NO_x (ppb). Note that the ordinate for NO concentrations is a logarithmic scale.

emission ratios from mobile sources (e.g., Fujita et al., 1992; Parrish et al., 2002). High vehicular traffic volumes and low BL heights in the morning tend to maximize pollutant concentrations. Morning NO_x and CO concentrations should remain largely unperturbed by photochemistry and should accurately reflect emission ratios from nearby sources, although long-range transport can enhance [CO]. NO_x emission from EGUs can confound the analysis, but since these emissions typically emanate from elevated stacks they should be transported aloft prior to the onset of convective mixing.

CO and NO_x concentrations measured during the morning rush hour (0500–0900 CST) from all wind directions and for all days of the

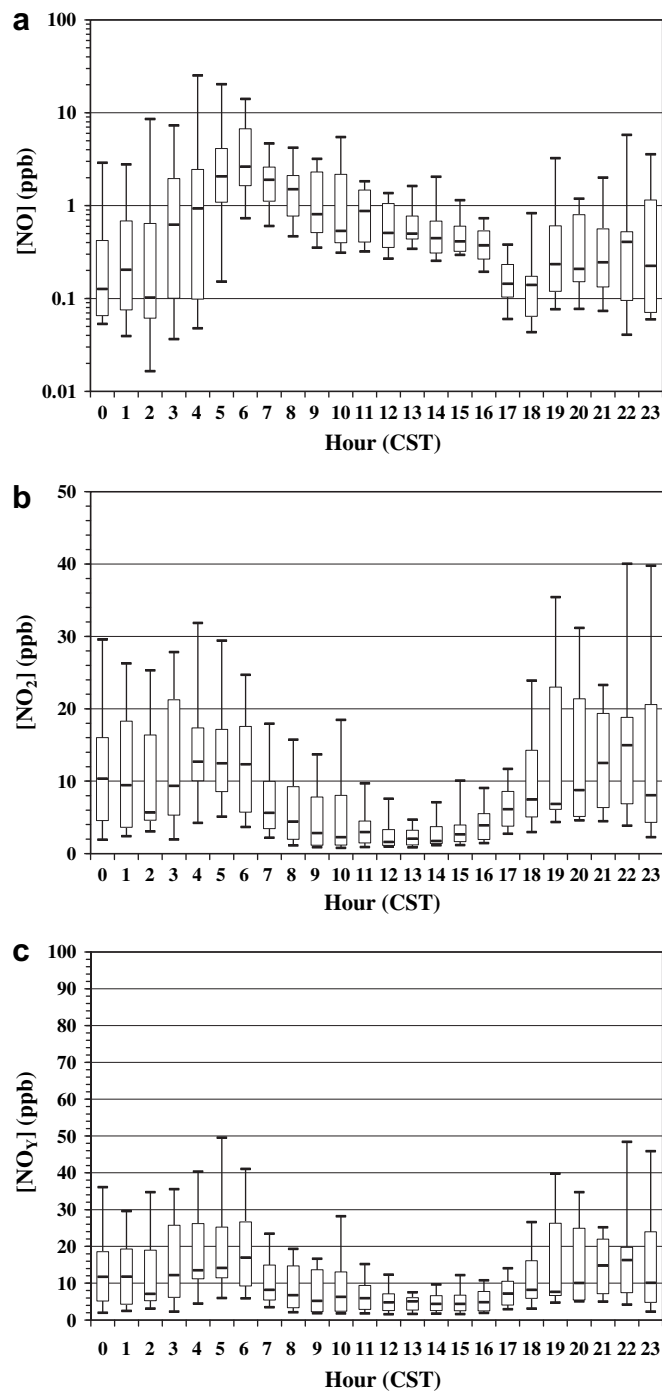


Fig. 5. Same as Fig. 2, for weekend data only: (a) NO (ppb), (b) NO₂ (ppb), (c) NO_x (ppb). Note that the ordinate for NO concentrations is a logarithmic scale.

TRAMP study are plotted in Fig. 6. The CO/NO_x emission ratio inferred from the fitted slope of a linear least squares regression is 5.81 ($r^2 = 0.8134$). The total uncertainty (0.94) in the calculated emission ratio is estimated by adding in quadrature the standard error of the fitted slope (0.31) and the combined uncertainties of the CO, NO, and NO₂ measurements discussed above. Our ratio agrees almost exactly with 2006 ratios computed from ambient monitoring stations in the Houston area (Cowling et al., 2007; Parrish et al., 2009). The CO/NO_x emission ratio determined from Moody Tower data reported by Parrish et al. (2009), 4.7, was calculated from an independent UH data set and included a relatively few observations of high [CO] and [NO_x]

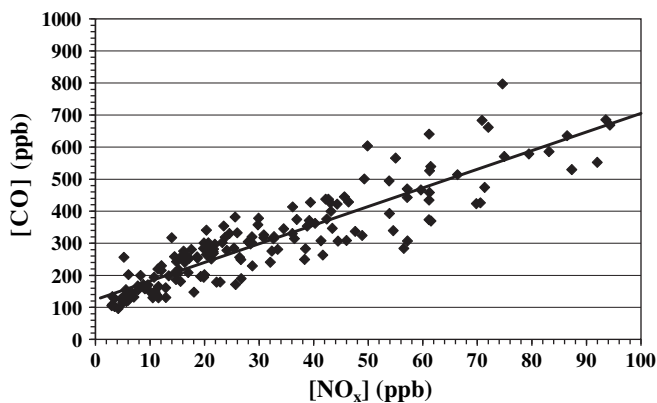


Fig. 6. Concentrations of CO and NO_x observed from 0500 to 0900 CST on all days of the TRAMP study. The solid line represents the fit of a least squares linear regression of the data, with a slope of 5.81 ± 0.94 ppb CO/ppb NO_x, and an intercept of 124 ppb CO ($r^2 = 0.8134$).

not detected by the NOAA instruments. Both the NOAA and UH NO_x instruments measured NO and NO₂ sequentially, so reported concentrations may suffer from increased uncertainties under rapidly fluctuating conditions. At NO_x concentrations below 70 ppb and under more quiescent conditions, CO/NO_x emission ratios derived from the two data sets agreed more closely (NOAA: 5.52, UH: 5.32).

3.5. Photochemical processing

Diurnal profiles of NO_x/NO_y ratios are presented in Fig. 7a. Concentrations of NO_z were calculated as the difference between NO_y and NO_x measurements; diurnal profiles are presented in Fig. 7b. (The designations NO_z and NO_y–NO_x shall be used interchangeably in the discussion below.) Approximately 4% of the total 1049 hourly observations of NO_z were slightly less than zero: 4 hourly observations were between –1 and –2 ppb, and 40 were between 0 and –1 ppb. NO_z concentrations of –0.41 to –1.26 ppb were sometimes calculated late at night or during the morning rush hour, while slightly negative [NO_z] (ca –0.05 ppb) occasionally resulted from uncertainties in the molybdenum converter artifact at NO_y concentrations of 1–2 ppb.

Median NO_x/NO_y ratios decreased through the morning and reached a minimum of approximately 0.63 near local solar noon (1300–1500 CST). Conversely, ratios of NO_z/NO_y were approximately 0.37 (median) and reached as high as 0.45–0.50 at the 25th percentile level at this time (Fig. 7c), with NO_z concentrations approaching 5 to as much as 10 ppb (Fig. 7b). Although high concentrations of O₃ and NO_z were often observed at the MT site, these measurements indicate that NO_x–O₃ photochemistry was far from exhausted, with substantial levels of NO_x still available for additional ozone generation farther downwind. NO_x/NO_y ratios increased during the evening and reached approximately 0.9 overnight, reflecting the persistence of NO_z species in the nighttime BL. Ratios approached unity in the morning rush hour when fresh injections of NO_x dominated the NO_y distribution.

Fig. 8 presents a diurnal profile of median ratios of measured component NO_y species to total NO_y. Median, 25th percentile, and 75th percentile concentrations for all reactive nitrogen species are listed in Table 2 for rush hour, midday, and overnight periods. Although NO_x constituted the majority of NO_y throughout the day, HNO₃ was the dominant NO_z species and constituted as much as 17–19.5% of NO_y from 1300 to 1500 CST. Median HNO₃ concentrations during midday (1100–1700 CST) were 1.531 ppb (central range 0.377–3.270 ppb). The pronounced peak in HNO₃ and HNO₃/NO_y near solar noon (Fig. 8) reflects the importance of the NO₂ + OH reaction as the dominant HNO₃ production pathway. HNO₃ accounted for about 3% of

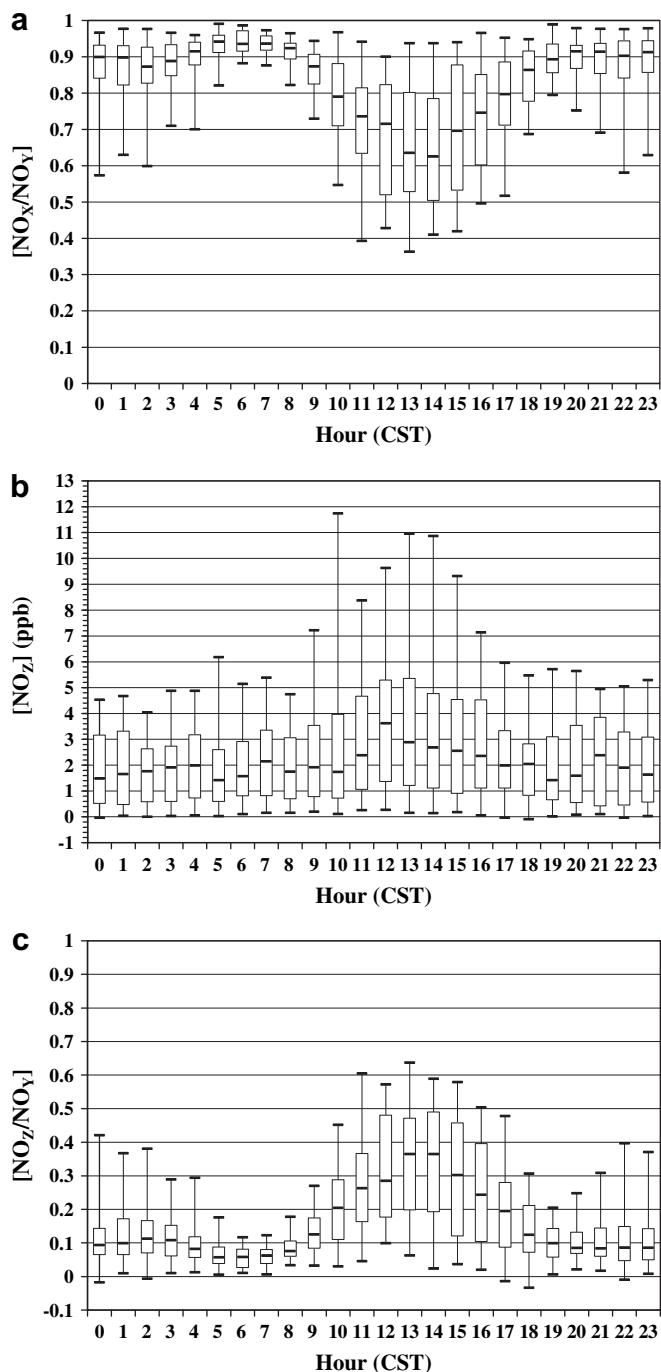


Fig. 7. Diurnal profiles of reactive nitrogen composition, as in Fig. 2, for all weekday and weekend data: (a) NO_x/NO_y, (b) [NO_z] (ppb), (c) NO_z/NO_y.

total NO_y at night, with a median concentration of 0.667 ppb from 2100 to 0500 (central range 0.141–1.197 ppb). Nighttime observations of aqueous NO₃⁻ in the MC technique were assumed to arise from either N₂O₅ (formed from the nighttime reaction of NO₂ and NO₃) or HNO₃ (formed from N₂O₅ hydrolysis in the gas and aerosol phase and from other heterogeneous reactions; Finlayson-Pitts and Pitts, 2000, and references therein).

Peroxyacyl nitrates comprised the second most abundant NO_z species, with median fractional contributions to NO_y of 2.3–3.1% at night and in the early morning (excluding rush hour), and 12.0–14.8% at midday (Fig. 8). The median concentration of PAN and PAN

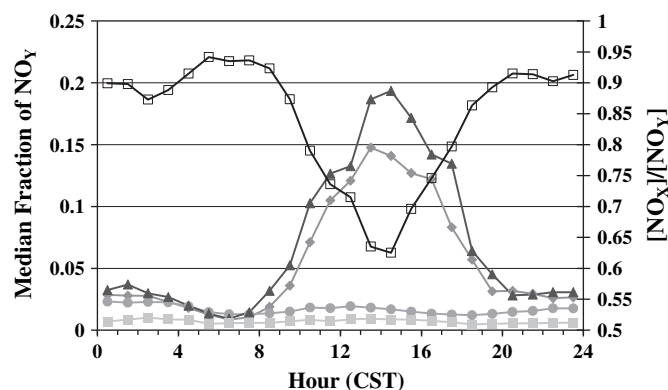


Fig. 8. Median fractions of the indicated NO_y species to NO_y as a function of time of day, calculated from diurnally aggregated concentrations: HNO_3/NO_y (solid triangles), PANs/NO_y (solid diamonds), HONO/NO_y (solid circles), $\text{p-NO}_3/\text{NO}_y$ (solid squares). NO_x/NO_y ratios (open squares) are keyed to right ordinate.

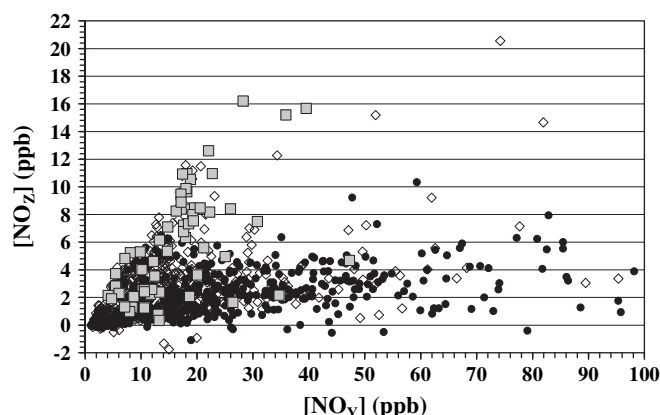


Fig. 9. Scatter plot of NO_z and NO_y concentrations (ppb) for day (0800–2000 CST; open diamonds) and night (2000–0800 CST; solid circles) periods, and for midday (1100–1700 CST) conditions under northeasterly flow (solid squares).

homologues was 0.289 ppb (central range 0.190–0.607 ppb) from 2100 to 0500 CST and increased to 0.907 (central range 0.454–1.962 ppb) throughout midday. PAN was by far the most abundant of the measured peroxyacyl nitrates. While contributions from PPN and MPAN were occasionally significant, PAN homologues were more often below the limit of detection (LOD: 30–40 ppt for PAN, PPN, and APAN; 85 ppt for PiBN, and 100 ppt for MPAN).

Concentrations and fractional contribution to NO_y by HONO and p-NO_3 were small. HONO formation is poorly understood. Gas phase formation by reaction of NO with OH proceeds only during the day, and the resulting HONO is rapidly photolyzed. At night HONO may arise from primary emissions from mobile sources (Pitts et al., 1984), or may be produced from heterogeneous reactions involving NO_2 (Finlayson-Pitts et al., 2003; Ammann et al., 1998). Median HONO concentrations were 0.347 ppb (central range 0.156–0.539 ppb, or about 1.5–2.2% of NO_y) overnight, but increased to 0.428 ppb (central range 0.214–0.700 ppb) in the morning rush hour, a rise attributed by Ziemba et al. (in this issue) to production of HONO by the heterogeneous conversion of HNO_3 on primary organic aerosols. Rapid photolysis decreased median HONO concentrations to 0.169 ppb (central range 0.106–0.251 ppb), or about 1–1.5% of NO_y during the day.

A scatter plot of NO_z and NO_y concentrations is presented in Fig. 9 for both day and night periods. As discussed above, daytime concentrations of NO_x and NO_y were highest in NE flow. Midday NE winds also contained the highest concentrations of NO_z species (Fig. 9), reflecting both the magnitude and reactivity of NO_x and VOC emissions in the HSC. Although not shown, the composition of this increased NO_z was dominated almost exclusively by HNO_3 and PANs; concentrations of HONO and p-NO_3 displayed no discernible increase in NE flow during the day or night. Ryerson et al. (2003) attributed higher PAN/ NO_y ratios in the Houston area to the high levels of reactive hydrocarbons in the HMA, and measured roughly

equal concentrations of HNO_3 and PAN compounds in aircraft transects of the HSC plume in 2000.

In order to investigate the dependence of NO_z species concentrations upon nearby source regions, we separated day and nighttime observations into 20° wind direction bins and calculated in each bin the median of the ratio of each species to NO_y . Results are shown in Fig. 10a (day) and 10b (night). Median ozone concentrations for each wind direction bin are also presented.

Large HNO_3/NO_y and PANs/ NO_y ratios in daytime NE flow implied by data in Fig. 9 are evident in Fig. 10a. Because HNO_3 and PANs were the dominant NO_z species in the HMA, both $[\text{NO}_z]$ and NO_z/NO_y were also largest in air masses impacted by sources in the HSC; ozone concentrations followed this pattern (Fig. 10a). These results are consistent with the findings of the earlier TEXAQS-2000 study (Ryerson et al., 2003; Daum et al., 2003, 2004) where high ozone concentrations and rates and efficiencies of ozone production observed in the HSC were attributed to the magnitude and reactivity of VOC and NO_x emission sources there. Aircraft flights in the 2006 TEXAQS-II campaign again confirmed the presence of large emission sources of NO_x and HRVOCs and the rapid and efficient production of O_3 in the HSC, followed by dispersion across the HMA (Cowling et al., 2007). Although data collected during TEXAQS-II suggest a reduction of approximately 40% in the emission of ethene and other HRVOCs from sources in the HSC (Cowling et al., 2007), our findings suggest that this region is still the source of maximum O_3 production in the HMA.

Fractional daytime contributions of PANs and HNO_3 to NO_y decreased in SE flow (140° – 160°), but increased slightly, along with ratios of HONO/ NO_y , in winds from the SSE-SW (160° – 220°). Fractional contribution of HNO_3 to NO_y was smaller than that of total PANs in southerly flow, in contrast to almost all other wind directions (Fig. 10a), perhaps due to adsorption of HNO_3 onto sea salt aerosols. The lack of significant enhancement of $\text{p-NO}_3/\text{NO}_y$ ratios in

Table 2

Trace gas concentrations (ppb) for select time periods.

Species	0500–0900 CST			1100–1700 CST			2100–0500 CST		
	Median	25th P'ile	75th P'ile	Median	25th P'ile	75th P'ile	Median	25th P'ile	75th P'ile
NO	6.741	1.860	16.785	0.953	0.527	1.571	0.188	0.074	1.238
NO_x	25.380	14.749	45.627	6.441	3.148	9.355	12.446	6.041	22.581
NO_y	26.408	15.785	46.670	9.766	5.198	15.928	14.581	7.560	24.942
HNO_3	0.519	0.154	0.830	1.531	0.377	3.270	0.667	0.141	1.197
PANs	0.265	0.169	0.473	0.907	0.454	1.962	0.289	0.190	0.607
HONO	0.428	0.214	0.700	0.169	0.106	0.251	0.347	0.156	0.539
p-NO_3	0.234	0.051	0.363	0.091	0.050	0.136	0.135	0.042	0.248

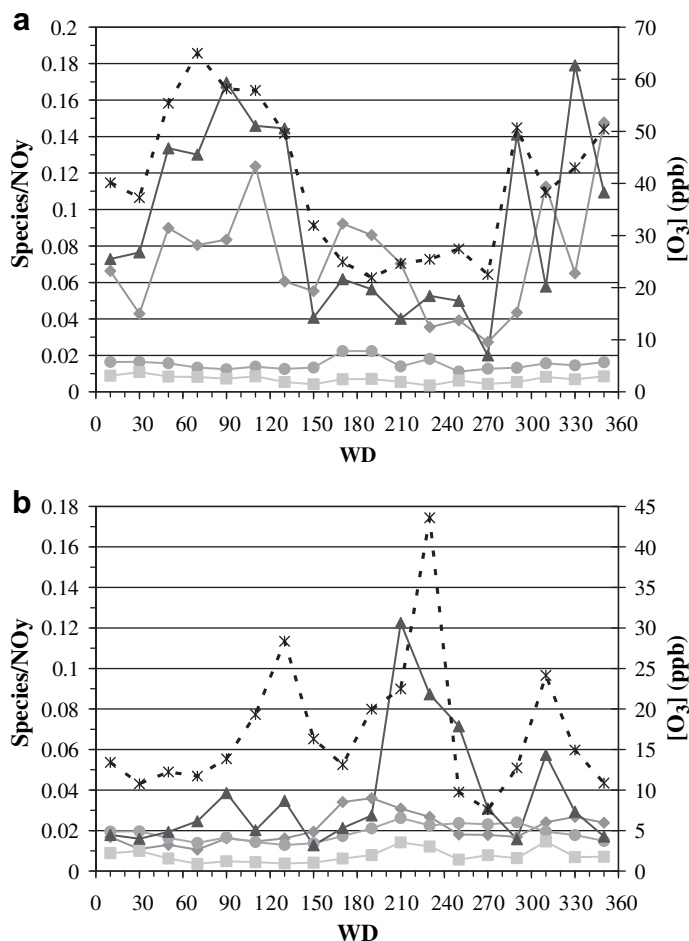


Fig. 10. Median ratio of select NO_y species to NO_y as a function of wind direction (20° bins) for: (a) day (0800–2000 CST) and (b) night (2000–0800 CST) periods. HNO_3/NO_y (solid triangles), PANs/NO_y (solid diamonds), HONO/NO_y (solid circles), and $\text{p-NO}_3^-/\text{NO}_y$ (solid squares). Median O_3 concentrations are denoted by a dashed line and are keyed to the right ordinate.

these air masses is not inconsistent with this interpretation, as the AMS responds only to fine mode non-refractory aerosols. Median daytime NO_z and NO_y concentrations were less than 0.70 ppb and 3.5 ppb, respectively, in this marine air.

Daytime fractions of PAN and HNO_3 increased in westerly to northerly flow, probably influenced by mobile source emissions (see Leuchner and Rappenglück, in this issue). However, daytime concentrations of NO_y and NO_z were lower in westerly-northerly flow than in winds from the NE, and median O_3 concentrations followed this pattern (Fig. 10a). Ratios of $\text{p-NO}_3^-/\text{NO}_y$ exhibited little variation with wind direction.

The variation of nighttime NO_z/NO_y ratios with wind direction was largely unremarkable (Fig. 10b), and ratios of NO_z species to NO_y were low, in accord with the shutdown of dominant photochemical processes at night. The most striking features of the nighttime data are the increases in O_3 and HNO_3/NO_y in winds from the ESE (100° – 140°), SW (200° – 260°), and NW (300° – 320°), suggesting the advection into the HMA of photochemically aged plumes. For further analysis we calculated backward trajectories using ARL's HYSPLIT (HYbrid Single-Particle Lagrangian Integrated Trajectory) model (Draxler and Hess, 1998; http://www.arl.noaa.gov/HYSPLIT_info.php) driven by 40 km resolution EDAS (Eta Data Assimilation System) meteorological data.

HYSPLIT back trajectories suggest that the highest O_3 concentrations (40–55 ppb) in nocturnal ESE flow were measured in air masses presumably impacted by petrochemical and other

industrial sources in coastal Louisiana during the previous 24 h period. However, on one occasion (Sept. 8) elevated O_3 concentrations in nighttime easterly flow were measured in air masses impacted by the Dallas-Fort Worth (DFW) area. Air masses influenced by the DFW area contained the highest O_3 concentrations measured in nighttime NW flow, although enhancements were also seen in parcels impacted by sources in Mexico.

Trajectories associated with four of six episodes of high nighttime or early morning HNO_3/NO_y ratios (ca 0.15) and O_3 concentrations in SW flow (Aug. 23–24, Aug 31–Sept 1, Sept. 1–2, Sept 26–27) demonstrated the recirculation of aged air previously impacted by the HMA or coastal Louisiana in the return flow of the land-breeze/gulf-breeze circulation. With the exception of Aug. 23–24, these episodes were also characterized by nighttime O_3 concentrations of 50–70 ppb. Back trajectories associated with the remaining two episodes (HNO_3/NO_y ca 0.15, O_3 ca 50–70 ppb on Sept. 6–7 and Sept. 13–14) suggested regional transport of polluted air masses from the north even though Sept. 6–7 was classified as a sea breeze day (Lefer et al., in this issue; Rappenglück et al., submitted for publication). It is possible that the 40 km EDAS model failed to resolve this fine scale recirculatory flow.

3.6. NO_y composition and budget

Hourly averaged concentrations of NO_y were compared to the sum of measured concentrations of individual NO_y components (NO_{y_i} : $\text{NO}_y = \text{NO}_x + \text{HNO}_3 + \text{PANs} + \text{HONO} + \text{p-NO}_3^-$). NO_x concentrations were measured with the solid-state photolytic converter described above. Hourly averaged concentrations of HNO_3 , PANs, HONO, and p-NO_3^- were calculated from 10-minute average data. Concentrations of PAN homologues reported to be below LOD were assumed to be half the stated LOD. AMS nitrate concentrations were converted to a mixing ratio equivalent assuming 298 K and 1 atm pressure. Nitrate radical (NO_3) concentrations measured with a long-path DOAS averaged only 11.0 ± 14.2 ppt (max 75.6 ppt) and 18.3 ± 20.6 ppt (max 98.2 ppt) from the lower and middle light paths, respectively (J. Stutz, personal communication), and were not considered. 697 h (338 day, 359 night) of data, covering approximately 60% of the total deployment period, were included in the analysis.

Results of the comparison between measured NO_y and NO_{y_i} are shown for day and nighttime periods in Fig. 11a and in expanded scale in Fig. 11b. A least squares linear regression of nighttime data yields the following equation: $\text{NO}_y(\text{ppb}) = ([\text{NO}_{y_i}](\text{ppb}) * 1.01) + 0.18$ ($r^2 = 0.9975$). During daylight hours, the corresponding regression equation changed to: $\text{NO}_y(\text{ppb}) = ([\text{NO}_{y_i}](\text{ppb}) * 1.03) - 0.42$ ($r^2 = 0.9933$). At low concentrations (Fig. 11b) measured $[\text{NO}_y]$ was larger than $[\text{NO}_{y_i}]$ at night, but smaller than $[\text{NO}_{y_i}]$ during the day. The total uncertainty in the fitted slope (0.16 day and night) is calculated by adding in quadrature the measurement uncertainties in NO_y ($\pm 10\%$) and NO_{y_i} ($\pm 12\%$, obtained by weighting the uncertainty in each measured species by its average fractional contribution to NO_y) with the standard error in the fitted slope ($\pm 0.26\%$ night, $\pm 0.45\%$ day). Overall, then, NO_y and NO_{y_i} concentrations agreed well to within the combined uncertainties of the measurement methods. Ryerson et al. (2003) demonstrated similar closure of the NO_y budget to within overall measurement uncertainties on all available flights of the WP-3D aircraft over Houston in 2000.

3.7. Budget of NO_x oxidation products (NO_z)

Because NO and NO_2 constituted the overwhelming fraction of NO_y during TRAMP ($77.4 \pm 17.1\%$ during the day; $89.2 \pm 10.3\%$ at night), the NO_y budget reflects primarily the measurement agreement for NO_x . A more stringent assessment should focus instead on the budget of NO_z compounds. Measurement uncertainties in NO,

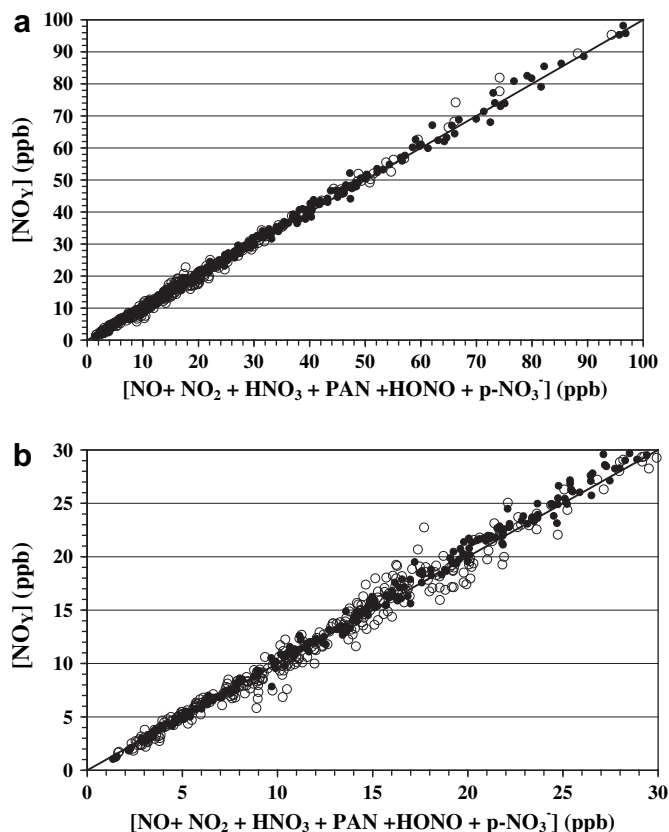


Fig. 11. Scatter plot of total NO_y concentrations (ppb) and the sum of NO_y components (NO_{y_i} ; ppb) for day (0800–2000 CST, open circles) and night (2000–0800 CST, solid circles) periods. A plot of the entire data set is presented in (a) and as an expanded scale in (b). The solid line denotes a 1:1 correspondence of the data. The equations of a linear least squares fit to the data are: ($[\text{NO}_y](\text{ppb}) = ([\text{NO}_{y_i}](\text{ppb}) * 1.03 \pm 0.16) - 0.42$; $r^2 = 0.9933$) for daytime data and ($[\text{NO}_y](\text{ppb}) = ([\text{NO}_{y_i}](\text{ppb}) * 1.01 \pm 0.16) + 0.18$; $r^2 = 0.9975$) at night.

NO_2 and NO_y can contribute substantially to overall uncertainty in NO_z , which is often calculated as a small difference between two large numbers. However, as reactive nitrogen species were measured with a common instrument and calibration standard, uncertainties associated with instrument calibration errors should affect measured NO_x and NO_y by similar magnitudes. Thus, overall uncertainties in NO_z are dominated by uncertainties in converter artifacts (0.040 ppb NO_x , 0.220 ppb NO_y) at low concentrations, and by variations in instrument sensitivity ($\pm 3\%$ for each channel) and conversion efficiencies ($\pm 3\%$ for NO_x , $\pm 1\%$ for NO_y based upon variations in GPT results) at higher NO_x and NO_y concentrations. The accuracy of NO_z determinations is therefore highest at midday, when NO_x/NO_y ratios are low, and degrades at night and in the morning rush hour.

In addition to random errors, calculated $[\text{NO}_z]$ may also suffer from systematic bias induced by interferences to either NO_x or NO_y detection. As discussed above, theoretical considerations suggest negligible interferences to the LED photolytic conversion technique. Conversion efficiencies of PAN, HNO_3 , HONO, and $p\text{-NO}_3^-$ on hot molybdenum were assumed to be equal to that of NO_2 (Joseph and Spicer, 1978; Grosjean and Harrison, 1985; Winer et al., 1974; Nunnermacker, 1990). Previous laboratory evaluations (unpublished data) have demonstrated the equivalency of NO_2 and HNO_3 reduction to NO on commercial converters. Conversion efficiencies of NH_3 and N_2O are negligible at an operating temperature of 350 °C (Fehsenfeld et al., 1987; Dickerson et al., 1984); NH_3 conversion was confirmed to be insignificant by testing the output of a certified permeation tube in the ARL laboratory.

Calculated NO_z concentrations are plotted against NO_{z_i} , the measured sum of [$\text{HONO} + \text{HNO}_3 + \text{PANs} + p\text{-NO}_3^-$] during day (1000–2000 CST) and night (2100–0500 CST) time periods in Fig. 12. Statistical descriptors of calculated $\text{NO}_z/\text{NO}_{z_i}$ ratios are presented in Table 3 for various time periods throughout the day. Because rapidly varying NO_x and NO_y concentrations can induce substantial errors in calculated NO_z , data collected during the morning rush hour and growth of the PBL (0500–1000 CST) were excluded from further analysis.

Despite the considerable scatter in the data, the plot in Fig. 12 suggests that the budget of NO_z compounds in the daytime data was generally closed to within the combined uncertainties of the techniques. Calculated concentrations of NO_z agreed well with the measured sum of NO_z components during the day: $[\text{NO}_z](\text{ppb}) = ([\text{NO}_{z_i}](\text{ppb}) * 1.01) + 0.044 \text{ ppb}$ ($r^2 = 0.8527$). The overall uncertainty in the daytime fitted slope, ± 0.30 , was calculated as the quadrature sum of the standard error of the fitted slope ($\pm 2.5\%$) plus uncertainties in NO_z and NO_{z_i} concentrations. Uncertainty in daytime NO_z concentrations ranged from an average of $\pm 175\%$ at NO_z concentrations below 1 ppb, to $\pm 44\%$ at 1–3 ppb, $\pm 25\%$ at 3–5 ppb, $\pm 18\%$ at 5–7 ppb, and $\pm 11\%$ at concentrations greater than 7 ppb. A median uncertainty of $\pm 28\%$ was assumed. Uncertainty in NO_{z_i} was calculated to be $\pm 11\%$ from the sum of the uncertainties of each measured component. Note that Stutz et al. (in this issue-a) deduced that daytime MC measurements of HONO may be plagued by interferences from photochemically produced species such as organic nitrites. Such compounds should also be converted to NO on hot molybdenum and pose no bias to $\text{NO}_z/\text{NO}_{z_i}$ ratios here, but daytime measurements of NO_z may include compounds not currently accounted for in species-specific measurements.

Despite greater uncertainty in nighttime NO_z concentrations, NO_z also agreed well with the sum of NO_{z_i} at night: $[\text{NO}_z](\text{ppb}) = ([\text{NO}_{z_i}](\text{ppb}) * 1.12) + 0.16 \text{ ppb}$ ($r^2 = 0.6899$) (Fig. 12). The overall uncertainty in the fitted slope was calculated to be ± 0.69 , reflecting the larger standard error of the slope ($\pm 4.7\%$) and the larger uncertainty in measured NO_z concentrations, which ranged from $\pm 165\%$ at concentrations less than 1 ppb, to $\pm 70\%$ at 1–3 ppb, $\pm 42\%$ at 3–5 ppb, and $\pm 32\%$ above 5 ppb. A median uncertainty of $\pm 61\%$ in the nighttime NO_z data was assumed.

While higher nighttime $\text{NO}_z/\text{NO}_{z_i}$ ratios may point to the presence of one or more unidentified photochemically labile NO_y species, they may well arise from competing errors or artifacts in NO_y

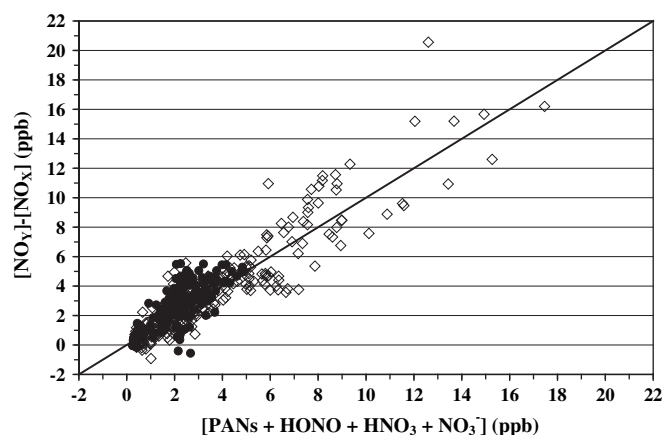


Fig. 12. Scatter plot of concentrations of NO_z and the sum of $\text{HNO}_3 + \text{PANs} + \text{HONO} + p\text{-NO}_3^-$ concentrations (ppb) for daytime (1000–2000; open circles) and nighttime (2100–0500 CST; solid circles) periods. Data collected from 0500 to 1000 CST were excluded. The solid line denotes a 1:1 correspondence of the data. The equations of a linear least squares fit to the data are: ($[\text{NO}_z](\text{ppb}) = ([\text{NO}_{z_i}](\text{ppb}) * 1.01 \pm 0.30) + 0.044 \text{ ppb}$; $r^2 = 0.8527$) during the day and ($[\text{NO}_z](\text{ppb}) = ([\text{NO}_{z_i}](\text{ppb}) * 1.12 \pm 0.69) + 0.16 \text{ ppb}$; $r^2 = 0.6899$) at night.

Table 3
Ratios of $\text{NO}_z/\text{NO}_{z_i}$ for select time periods.

	$\text{NO}_z/\text{NO}_{z_i}$			
	Day	Night	Dark	MidDay
	0800–2000 CST	2000–0800 CST	2100–0500 CST	1100–1700 CST
Average	1.053	1.275	1.189	1.029
Std. Deviation	0.516	0.569	0.528	0.496
Median	1.042	1.226	1.179	0.973
5th Percentile	0.199	0.460	0.225	0.216
25th Percentile	0.788	0.948	0.939	0.789
75th Percentile	1.286	1.519	1.467	1.247
95th Percentile	1.977	2.197	1.938	1.788

measurement and changes in NO_y composition from day to night. In any case, the small differences observed in day/night $\text{NO}_z/\text{NO}_{z_i}$ ratios inferred from the regressions above are well within the combined measurement uncertainties of the analytical methods and are not statistically significant. Therefore, the data must be compared with caution and any interpretation will remain speculative.

Diurnal profiles of $\text{NO}_z/\text{NO}_{z_i}$ ratios (excluding data from 0500 to 1000 CST) are presented in Fig. 13. Diurnally averaged solar zenith angles calculated at the location of the Moody Tower appear as a solid line. Median ratios of $\text{NO}_z/\text{NO}_{z_i}$ were very near to unity during the day, began to increase after sunset, and increased throughout the night to reach a maximum at 0300–0500 CST. Median values of the difference ($[\text{NO}_z]-[\text{NO}_{z_i}]$) ranged from 0.15 to 0.35 ppb at night and increased to ca 0.50 ppb at 0400–0500 CST. HNO_3/NO_y and PANs/NO_y ratios were not very different between early evening and early morning time periods, however, suggesting that measurement artifacts may not have played a significant role in increases in observed $\text{NO}_z/\text{NO}_{z_i}$ ratios. This is also demonstrated by data in Fig. 14, a plot of day and night $\text{NO}_z/\text{NO}_{z_i}$ ratios as a function of NO_x/NO_y ratios; nighttime data exhibit slightly greater (though not significant) discrepancies between NO_z and NO_{z_i} ratios than daytime values at equivalent NO_x fractions.

Hourly $\text{NO}_z/\text{NO}_{z_i}$ ratios were evaluated on an individual basis, and those hours for which differences between NO_z and the sum of NO_{z_i} exceeded the combined measurement uncertainties were examined more closely. In the daytime a total of 31 h were recorded in which the sum of NO_{z_i} exceeded NO_z by an amount greater than the combined measurement uncertainties (case 1); 29 h saw $\text{NO}_z \gg \text{NO}_{z_i}$ (case 2). In general, conditions were similar (NO_y concentrations of 1–20 ppb, SO_2 concentrations of 0–12.5 ppb, and CO concentrations of approximately 90–270 ppb) for case 1 and case 2 events, implying that

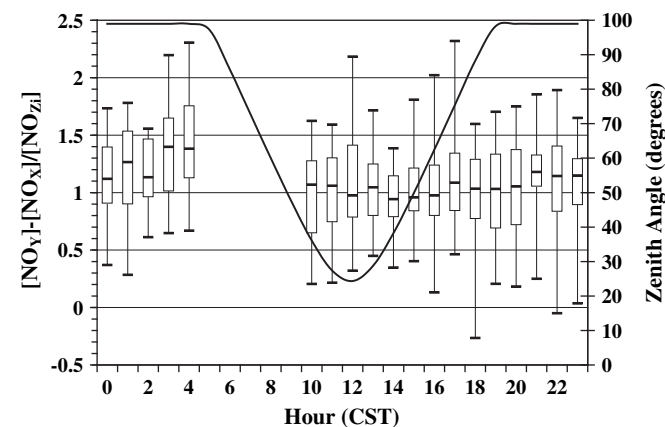


Fig. 13. Same as Fig. 2, for $\text{NO}_z/\text{NO}_{z_i}$ ratios. Data collected from 0500 to 1000 CST were excluded. The solid line represents the calculated median zenith angle during the study period.

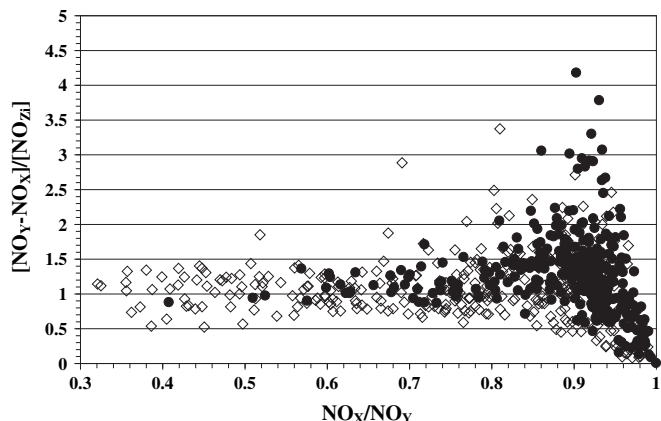


Fig. 14. $\text{NO}_z/\text{NO}_{z_i}$ ratios as a function of NO_x/NO_y ratios for daytime (0800–2000 CST; open circles) and nighttime (2000–0800 CST; solid circles) periods.

random errors were responsible for the $\text{NO}_z/\text{NO}_{z_i}$ discrepancies. Correlations (not shown) between the difference ($\text{NO}_z-\text{NO}_{z_i}$) and secondary species (O_3 , $\text{HNO}_3/\text{NO}_{z_i}$) were poor, as NO_z concentrations were sometimes significantly greater or less than the sum of NO_{z_i} at equivalent ozone concentrations. At higher primary pollutant loads in the daytime ($[\text{NO}_y] > 20$ ppb, $[\text{SO}_2] > 13$ ppb, $[\text{CO}] > 270$ ppb) NO_z only exceeded NO_{z_i} ; the reverse was never noted.

At night, 11 h were noted in which $\text{NO}_z \gg \text{NO}_{z_i}$; NO_z was never significantly less than the sum of NO_{z_i} . The difference ($\text{NO}_z-\text{NO}_{z_i}$) correlated poorly with virtually every indicator or diagnostic variable discussed above, including wind direction, with the exception of O_3 ; a negative correlation was noted ($r^2 = 0.4999$), so that ($\text{NO}_z-\text{NO}_{z_i}$) differences were smaller at higher $[\text{O}_3]$. NO_z exceeded NO_{z_i} to greater extent under conditions of high NO_x and NO_y concentrations, and at higher NO_x/NO_y fractions.

While large uncertainties inherent in NO_z calculations prevent any statistically meaningful interpretation of the data, and any explanations must therefore remain speculative, our results are consistent with the recent findings of Osthoff et al. (2008), who reported the measurement of nitryl chloride (ClNO_2) in the nocturnal Houston BL as part of the TEXAQS-II campaign. Our observations of nighttime $\text{NO}_z/\text{NO}_{z_i}$ ratios are consistent with the nocturnal formation and daytime photolysis of this labile species, and median differences between NO_z and NO_{z_i} concentrations are in general agreement with reported ClNO_2 concentrations (Osthoff et al., 2008). ClNO_2 formation proceeds through the heterogeneous interaction of N_2O_5 with chloride-containing aerosols, and our results suggest greater discrepancy in the NO_z budget under conditions in which high N_2O_5 may be expected.

Other and/or additional nitrogen species may also contribute to $\text{NO}_z/\text{NO}_{z_i} > 1$ at night in the HMA. NO_3 radical concentrations were ignored in the NO_z budget analysis above and accounted for only 10–20 ppt of NO_z on average, much smaller than the nighttime $\text{NO}_z/\text{NO}_{z_i}$ discrepancy (median: 0.15–0.50 ppb). Reaction with isoprene, isobutene, and 1,3-butadiene comprised the dominant loss mechanism for NO_3 in the nocturnal Houston BL (Stutz et al., in this issue-b), and secondary N-containing organic species formed in these reactions could enhance measured NO_z concentrations. Pernitric acid (HO_2NO_2) is also a potential contributor to the $\text{NO}_z/\text{NO}_{z_i}$ imbalance but would likely be measured to some extent as NO_2 or NO_3 in the MC technique.

4. Summary

Concentrations of CO, SO_2 , NO, NO_2 , and NO_y were measured atop the University of Houston's Moody Tower supersite during the 2006 TRAMP study, and their temporal variations reflected the interactions of multiple local sources characteristic of a large urban

environment. SO₂ concentrations were usually low, but increased dramatically at midday in sporadic plume events from sources in the HSC. Winds from the SW brought emissions from EGUs (W. A. Parish) into the HMA during daytime. The lowest concentrations of all primary and secondary species were observed in clean marine air in southerly flow. Concentrations of CO and NO_x displayed large diurnal variations in keeping with their co-emission by mobile sources in the HMA. A CO/NO_x emission ratio of 5.81 ± 0.94 was inferred from consideration of morning rush hour data.

Nighttime concentrations of NO_x and NO_y were highest in winds from the NNW-NE due to emission from mobile sources in the morning rush hour. Median ratios of NO_x/NO_y were approximately 0.9 overnight, reflecting the persistence and/or generation of NO_z species in the nighttime Houston BL, and approached unity in the morning rush hour, when fresh emissions of NO_x dominated the NO_y budget. Daytime concentrations of NO_x and NO_y were highest in winds from the HSC to the NE. Occasional late-night and early morning releases of NO were observed in winds from the HSC, perhaps from refinery flares and/or emission from ships. NO_x/NO_y ratios reached their minimum values (median ca 0.63) from 1300 to 1500 CST, and air masses often retained enough NO_x to sustain additional O₃ formation farther downwind. HNO₃ and PANs comprised the dominant NO_z species in the HMA, representing, on a median basis, 17–20% and 12–15% of NO_y, respectively, at midday. Contributions from HONO and p-NO₃⁻ were far smaller. Concentrations of HNO₃, PANs, and NO_z, and fractional contributions of these species to NO_y were at a maximum in NE flow, reflecting the source strength and reactivity of precursor emissions in the HSC. As a result, daytime O₃ concentrations were highest in air masses with HSC influence. Overall our findings confirm the impact of the HSC as a dominant source region within the HMA.

Variations of nighttime NO_z/NO_y ratios with wind direction were largely unremarkable, but increases in O₃ and HNO₃/NO_y were noted in winds from the ESE (100°–140°), SW (200–260°), and NW (300–320°), suggesting the advection into the HMA of photochemically aged plumes. ARL's HYSPLIT model was used to calculate back trajectories and confirmed the recirculation of these parcels either over the HMA or nearby coastal Louisiana. In some instances, back trajectories suggested the transport of aged air masses from the DFW area as well as from Mexico.

A comparison of total NO_y measurements with the sum of measured NO_y species, NO_{yi}, yielded excellent overall agreement during both day (NO_y(ppb) = ([NO_{yi}](ppb)*1.03 ± 0.16) – 0.42; r² = 0.9933) and night (NO_y(ppb) = ([NO_{yi}](ppb)*1.01 ± 0.16) + 0.18; r² = 0.9975). A similar comparison between NO_y–NO_x concentrations and the sum of NO_z species, NO_{zi}, also yielded good overall agreement despite the increased uncertainty inherent in calculated NO_z concentrations. NO_z/NO_{zi} ratios increased to approximately 1.2 overnight, a difference of 0.15–0.50 ppb. While not statistically different from unity, nighttime NO_z/NO_{zi} ratios were consistent with the presence of photochemically labile NO_y species, and the magnitude of NO_z–NO_{zi} differences was generally consistent with recent observations of ClNO₂ in the nocturnal Houston BL.

Acknowledgments

The authors would like to express their gratitude to the Houston Advanced Research Center (HARC) and the Texas Commission on Environmental Quality (TCEQ) for supporting and funding this research. We would also like to thank Dr. Jochen Stutz (UCLA) for providing us with the DOAS data sets. Ms. Marcia Wood (NOAA/ARL) provided extensive support for travel, logistical, and budget considerations. Mention of commercial brands, manufacturer, or supplier does not imply or constitute official endorsement by the

National Oceanic and Atmospheric Administration, Department of Commerce, or United States government.

References

- Ammann, M., Kalberer, M., Jost, D.T., Tobler, L., Rossler, E., Piguet, D., Gaggeler, H.W., Baltensperger, U., 1998. Heterogeneous production of nitrous acid on soot in polluted air masses. *Nature* 395 (6698), 157–160.
- Buhr, M.P., Parrish, D.D., Norton, R.B., Fehsenfeld, F.C., Sievers, R.E., Roberts, J.M., 1990. Contribution of organic nitrates to the total reactive nitrogen budget at a rural eastern U.S. site. *J. Geophys. Res.* 95, 9809–9816.
- Cowling, E.B., Furiness, C., Dimitriades, B., Parrish, D., 2007. Final Rapid Science Synthesis Report: findings from the Second Texas Air Quality Study (TexAQ5 II) Draft Report to TCEQ Contract number 582-4-65614.
- Daum, P.H., Kleinman, L.L., Springston, S.R., Nunnermacker, L.J., Lee, Y.-N., Weinstein-Lloyd, J., Zheng, J., Berkowitz, C., 2003. Origin and properties of O₃ formation in the Houston urban and industrial plumes during the TEXAQ5 2000 study. *J. Geophys. Res.* 108, 4715. doi:10.1029/2003JD003552.
- Daum, P.H., Kleinman, L.L., Springston, S.R., Nunnermacker, L.J., Lee, Y.-N., Weinstein-Lloyd, J., Zheng, J., Berkowitz, C., 2004. Origin and properties of plumes of high ozone observed during Texas 2000 Air Quality Study (TEXAQ5 2000). *J. Geophys. Res.* 109, D17306. doi:10.1029/2003JD004311.
- Day, B.M., Rappenglück, B., Clements, C.B., Tucker, S.C., Brewer, W.A. Characteristics of the nocturnal boundary layer in Houston, Texas during TEXAQ5-II, in this issue.
- Dickerson, R.R., Delany, A.C., 1988. Modification of a commercial gas filter correlation CO detector for enhanced sensitivity. *J. Atmos. Ocean. Tech.* 5, 424–431.
- Dickerson, R.R., Delany, A.C., Wartburg, A.F., 1984. Further modification of a commercial NO_x detector for high sensitivity. *Rev. Sci. Instrum.* 55 (12), 1995–1998.
- Draxler, R.R., Hess, G.D., 1998. An overview of the Hysplit_4 modeling system for trajectories, dispersion, and deposition. *Aust. Met. Mag.* 47, 295–308.
- Fahey, D.W., Hübler, G., Parrish, D.D., Williams, E.J., Norton, R.B., Ridley, B.A., Singh, H.B., Liu, S.C., Fehsenfeld, F.C., 1986. Reactive nitrogen species in the troposphere: measurements of NO, NO₂, HNO₃, particulate nitrate, peroxyacetyl nitrate (PAN), O₃, and total reactive odd nitrogen (NO_y) at Niwot Ridge, Colorado. *J. Geophys. Res.* 91, 9781–9793.
- Fehsenfeld, F.C., Dickerson, R.R., Hubler, G., Luke, W.T., Nunnermacker, L.J., Williams, E.J., Roberts, J.M., Calvert, J.G., Curran, C.M., Delany, A.C., Eubank, C.S., Fahey, D.W., Fried, A., Gandrud, B.W., Langford, A.O., Murphy, P.C., Norton, R.B., Pickering, K.E., Ridley, B.A., 1987. A ground-based intercomparison of NO, NO_x, and NO_y measurement techniques. *J. Geophys. Res.* 92, 14,710–14,722.
- Finlayson-Pitts, B.J., Pitts Jr., J.N., 2000. Chemistry of the Upper and Lower Atmosphere: Theory, Experiments, and Applications. Academic Press, San Diego, CA, 969 pp.
- Finlayson-Pitts, B.J., Wingen, L.M., Sumner, A.L., Syomin, D., Ramazan, K.A., 2003. The heterogeneous hydrolysis of NO₂ in laboratory systems and in outdoor and indoor atmospheres: an integrated mechanism. *Phys. Chem. Chem. Phys.* 5 (2), 223–242.
- Flynn, J., Lefer, B., Rappenglück, B., Leuchner, M., Perna, R., Dibb, J., Ziemba, L., Anderson, C., Stutz, J., Brune, W., Ren, X., Mao, J., Luke, W., Olson, J., Chen, G., Crawford, J. Impact of clouds and aerosols on Ozone production in Southeast Texas, in this issue.
- Fujita, E.M., et al., 1992. Comparison of emission inventory and ambient concentration ratios of CO, NMOG, and NO_x in California's South Coast air basin. *J. Air Waste Manag. Assoc.* 42 (3), 264–276.
- Grosjean, D., Harrison, J., 1985. Response of chemiluminescent NO_x analyzers and ultraviolet ozone analyzers to organic air pollutants. *Environ. Sci. Technol.* 19, 862–865.
- Jiang, G., Fast, J.D., 2004. Modeling the effects of VOC and NO_x emission sources on ozone formation in Houston during the TexAQ5 2000 field campaign. *Atmos. Environ.* 38, 5071–5085.
- Joseph, D.W., Spicer, C.W., 1978. Chemiluminescence method for atmospheric monitoring of nitric acid and nitrogen oxides. *Anal. Chem.* 50, 1400–1403.
- Kleinman, L.L., Daum, P.H., Imre, D., Lee, Y.-N., Nunnermacker, L.J., Springston, S.R., Weinstein-Lloyd, J., Rudolph, J., 2002. Ozone production rate and hydrocarbon reactivity in 5 urban areas: a cause of high ozone concentrations in Houston. *Geophys. Res. Lett.* 29, 1467. doi: 10.1029/2001GL014569.
- Lack, D., Lerner, B., Granier, C., Baynard, T., Lovejoy, E., Massoli, P., Ravishankara, A.R., Williams, E., 2008. Light absorbing carbon emissions from commercial shipping. *Geophys. Res. Lett.* 35, L13815. doi:10.1029/2008GL033906.
- Lefer, B., Rappenglück, B., Flynn, J., Haman, C. Photochemical and meteorological climate during the Texas-II Radical and Aerosol Measurement Project (TRAMP), in this issue.
- Leuchner, M., Rappenglück, B. VOC Source-Receptor Relationships in Houston during TexAQ5-II, in this issue.
- Luke, W.T., 1997. Evaluation of a commercial pulsed fluorescence detector for the measurement of low-level SO₂ concentrations during GASIE. *J. Geophys. Res.* 102, 16,255–16,265.
- Luke, W.T., Arnold, J.R., Gunter, R.L., Watson, T.B., Wellman, D.L., Dasgupta, P.K., Li, J., Riemer, D., Tate, P., 2007. The NOAA Twin Otter and its role in BRACE: platform description. *Atmos. Environ.* 41, 4177–4189.
- Neuman, J.A., Huey, L.G., Dissly, R.W., Fehsenfeld, F.C., Flocke, F., Holecek, J.C., Holloway, J.S., Hübler, G., Jakoubek, R., Nicks Jr., D.K., Parrish, D.D., Ryerson, T.B., Sueper, D.T., Weinheimer, A.J., 2002. Fast-response airborne in situ measurements of HNO₃ during the Texas 2000 air quality study. *J. Geophys. Res.* 107 (D.20), 4436. doi:10.1029/2001JD001437.

- Nunermacker, L.J., 1990. Calibration and Detection of Reactive Nitrogen Compounds in the Atmosphere. Ph.D. dissertation. Department of Chemistry, University of Maryland, College Park, MD.
- Osthoff, H.D., et al., 2008. Unexpectedly high ClNO₂ mixing ratios in the polluted subtropical marine boundary layer. *Nat. Geosci.* 1, 324–328.
- Parrish, D.D., Holloway, J.B., Fehsenfeld, F.C., 1994. Routine, continuous measurement of carbon monoxide with parts per billion precision. *Environ. Sci. Technol.* 28, 1615–1618.
- Parrish, D.D., et al., 2002. Decadal change in carbon monoxide to nitrogen oxide ratio in US vehicular emissions. *J. Geophys. Res.* 107 (D12), 4140. doi:10.1029/2001JD000720.
- Parrish, D.D., et al., 2009. Overview of the Second Texas Air Quality Study (TexAQSS II) and the Gulf of Mexico Atmospheric Composition and Climate Study (GoMACCS). *J. Geophys. Res.* 114 D00F13, doi:10.1029/2009JD011842.
- Pitts, J.N., Biermann, H.W., Winer, A.M., Tuazon, E.C., 1984. Spectroscopic identification and measurement of gaseous nitrous acid in direct auto exhaust. *Atmos. Environ.* 18, 847–854.
- Rappenglück, B., Alvarez, S., Buhr, M., Byun, D., Czader, B., Dasgupta, P., Estes, M., Kim, S., Leuchner, M., Li, Q., Luke, W., In-situ ground-based and airborne formaldehyde measurements during the TRAMP study, *Environ. Sci. Technol.*, submitted for publication.
- Ridley, B.A., Carroll, M.A., Gregory, G.L., Sachse, G.W., 1988. NO and NO₂ in the troposphere: Technique and measurements in regions of a folded tropopause. *J. Geophys. Res.* 93 (D12), 15,813–15,830.
- Ryerson, T.B., et al., 2003. Effect of petrochemical industrial emissions of reactive alkenes and NO_x on tropospheric ozone formation in Houston, Texas. *J. Geophys. Res.* 108, 4249. doi:10.1029/2002JD003070.
- Stedman, D.H., 1976. A flow independent procedure for the gas phase titration of an ozone source. *J. Air Pollut. Control Assoc.* 26, 62.
- Stutz, J., Oh, H.-J., Whitlow, S.I., Anderson, C., Dibb, J.E., Lefer, B.L., Rappenglück, B., Flynn, J.H. Intercomparison of DOAS and mist-chamber IC measurements of HONO in Houston, TX, in this issue-a.
- Stutz, J., Wong, K.W., Lawrence, L., Flynn, J.H., Rappenglück, B., Lefer, B., Brune, W., Ziemba, L., Griffin, R. Nocturnal NO₃ radical chemistry in Houston, TX, in this issue-b.
- Williams, E.J., Roberts, J.M., Baumann, K., Bertman, S.B., Buhr, S., Norton, R.B., Fehsenfeld, F.C., 1997. Variations in NO_y composition at Idaho Hills, Colorado. *J. Geophys. Res.* 102, 6297–6314.
- Williams, E.J., Lerner, B.M., Murphy, P.C., Herndon, S.C., Zahniser, M.S. Emissions of NO_x, SO₂, CO, H₂CO and C₂H₄ from commercial marine shipping during TexAQSS 2006. *J. Geophys. Res.*, in press.
- Winer, A.M., Peters, J.W., Smith, J.P., Pitts Jr., J.N., 1974. Response of commercial chemiluminescent NO–NO_x analyzers to other nitrogen-containing compounds. *Environ. Sci. Technol.* 8, 1118–1121.
- Ziemba, L.D., Dibb, J.E., Griffin, R.J., Anderson, C.H., Whitlow, S.I., Lefer, B.L., Rappenglück, B., Flynn, J.H. Heterogeneous conversion of nitric acid to nitrous acid on the surface of primary organic aerosol in an urban atmosphere, in this issue.